Hindawi
International Journal of Antennas and Propagation
Volume 2018, Article ID 5695987, 8 pages
https://doi.org/10.1155/2018/5695987

Research Article

A Thin and Broadband Linear-to-Circular Polarizer Based on Grid-Patch Structure for Ku-Band

Hao-ming Hu, Dong-fang Zhou, Xue Lei, and Jun-mo Wu

National Digital Switching System Engineering and Technological R&D Center, Zhengzhou 450002, China

Correspondence should be addressed to Hao-ming Hu; hhmseu2012@163.com

Received 13 September 2018; Revised 8 November 2018; Accepted 12 November 2018; Published 13 December 2018

Academic Editor: Francisco Falcone

A three-layer circular polarization selective surface operating in Ku-band is proposed in this communication. We design a thin grid-patch structure to achieve linear-to-circular polarization transformation over a wide frequency band. The periodic structure could be analyzed via equivalent circuit model theory. Numerical simulations have been carried out and the prototype structures have been fabricated and experimentally validated. The axial ratio (AR) of the transmitted field remained below 3 dB over the entire bandwidth, and the 3 dB AR bandwidth is approximately 44.6%. The design has a subwavelength thickness of 6 mm ($0.28\lambda_c$). Besides, this design could be also applied to beam scanning antennas because of its capability in condition of large oblique incidence angle (±50 deg).

1. Introduction

In recent years, with the rapid development of communication technologies, the range of antenna applications has become wider and the demand for communication under different propagation environment has become higher. Thus, single polarization mode of electromagnetic waves can no longer meet the requirements.

Nowadays, linear-to-circular polarization converter based on frequency selective surface (FSS) has been studied extensively and how to achieve large angle of incidence is significant in beam scanning antenna. Most often, polarization control is achieved with a quarter-wave plate which is one or several layers and the common structure is meander line [1]. In [2], Fei et al. proposed a novel single-layer linear-to-circular polarizer consisting of hybrid meander line and loop configuration. Although it is characterized by wide band, its insertion loss exceeds 3 dB. Also, other single-layer structures such as cross slot [3] and split slot ring [3] are difficult to achieve broadband and low loss at the same time. To solve this problem, multilayer CPFSS structures become a hot research point [4]. Momeni Hasan Abadi and Behdad proposed the concept of a miniaturized-element frequency selective surface (MEFSS) [5] that provides a stable frequency response for 40% 3 dB AR bandwidth and oblique incidence angles during ±45 degrees (low insertion loss). An approach focusing on designing multilayer polarizer was presented by Blanco and Sauleau in [6]. His design (five metasurface layers) could achieve wide axial ratio bandwidth of 19.6% for 50 degrees of incidence. Up to now, the maximum degree of incidence is 70 [7] which uses five layers. But its bandwidth is narrow, only 4.8% in 8–8.4 GHz. However, the overall thickness of these designs is electrically large. Thus, two [8, 9] or three layers [10, 11] play a much more important role in linear-to-circular polarizer designing and three-layer structure is considered as the minimum number of layers that is possible to provide perfect transmission and complete phase coverage. Increasing or reducing the number of layers could not meet the demand of performance and cost.

Considering three is the most appropriate number of layers, in this paper, a three-layer linear-to-circular polarizer is proposed and the structure of grid-patch is efficient

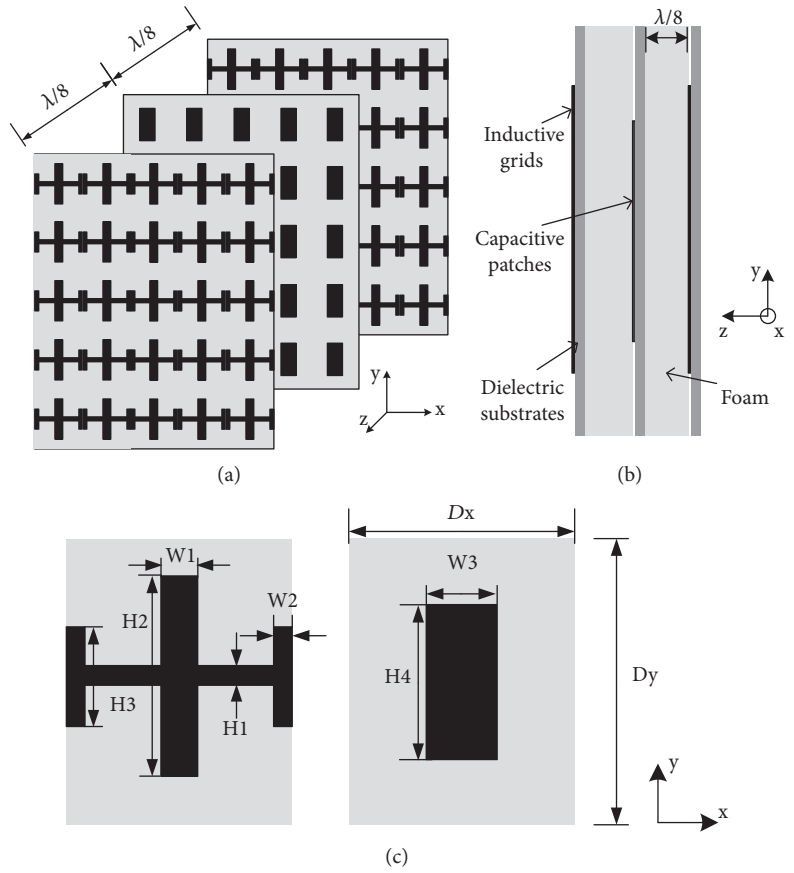

Figure 1: (a) The three-dimension (3D) topology of the proposed FSS. (b) The side view of the unit cell. (c) Unit cells of grid and patch surfaces with the definitions of their dimensions (see Table 1).

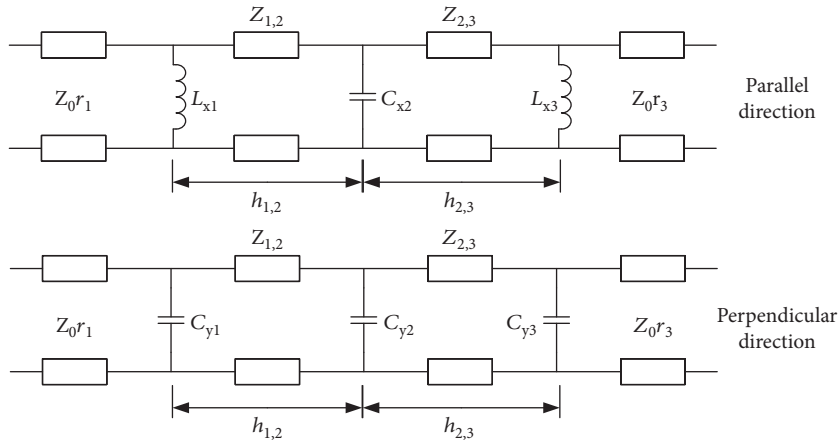

Figure 2: Equivalent circuit model of the proposed FSS structure.

in polarization transformation. It is characterized by wide bandwidth (44.6%) and low profile ($0.28\lambda_c$). Moreover, it is suitable to be applied to beam scanning antenna (±50 degrees of incidence) [12].

The rest of this communication is organized as follows. Section 2 describes the configuration and design principle of the proposed linear-to-circular polarizer. In Section 3, simulated and measured results of the designed polarizer are presented. Finally, a brief summary is given in Section 4.

2. Description of the Proposed Structure

2.1. Geometry. Design and operating principle will be analyzed in this section. It should be noted that a necessary condition for achieving high transmission efficiency is

Table 1: Parameters of the equivalent circuit.

Parameter	L_{x1}	C_{x2}	L_{x3}	$h_{1,2}$	$h_{2,3}$
Value	198.0 pH	342.0 pH	235.0 pH	2.5 mm	2.5 mm
Parameter	$Z_{1,2}$	$Z_{2,3}$	C_{y1}	C_{y2}	C_{y3}
Value	13.09 Ω	13.09 Ω	176.0 fF	383.0 fF	169.0 fF

Table 2: Optimal parameters of the FSS structure.

Parameter	D_x	D_y	W_1	W_2	W_3
Value	7.5 mm	9 mm	1.2 mm	0.5 mm	2.3 mm
Parameter	H_1	H_2	H_3	H_4	
Value	0.5 mm	5 mm	4 mm	4.6 mm	

that the quarter-wave plate must be symmetric, thus requiring the outer sheets to be identical [10]. Considering about this principle, the three-dimension (3D) topology of the proposed FSS is shown in Figures 1(a) and 1(b). It consists of a three-layer structure and each layer is composed of metal layer, dielectric substrates (F4B, thickness = 0.254 mm, $\varepsilon_r = 2.2$, $\tan\delta = 0.001$), and foam, which is Rohacell 71HF ($\varepsilon_r = 1.1$). The glue used to stick all the layers together has a permittivity of $\varepsilon_r = 3.5$, a loss tangent of $\tan\delta = 0.0015$. Each metal layer is a two-dimensional (2-D) planar periodic structure. The top metal layer is inductive grid structure and the middle layer is capacitive patch, while the bottom layers can be inductive or capacitive depending on the polarization. Figure 1(b) shows the side view of the structure. The geometry of unit cell is shown in Figure 1(c).

When a linearly polarized incident wave E^i, titled 45 degrees relative to x and y directions, transmits to the surface of polarizer, the incident wave can be decomposed to obtain two orthogonal electromagnetic components with the same amplitude and the same phase in the vertical direction ($\vec{E}_\perp$) and the horizontal direction ($\vec{E}_\parallel$). The expression of the incident wave is

$$\vec{E}^i = \vec{E}_\perp + \vec{E}_\parallel = E_0\left(\vec{e}_\perp + \vec{e}_\parallel\right)e^{-jkz}, \quad (1)$$

where E_0 is the electric field amplitude of the incident wave and $\vec{e}_\perp$ and $\vec{e}_\parallel$ are the unit vectors in the vertical and horizontal directions, respectively.

Within the operational band, the magnitude of the transmission coefficient for each component is ideally equal to one and the device passes both components very efficiently within the pass band with little or no attenuation. Due to the polarization converter has different frequency responses for these two components, the incident wave can be also expressed by:

$$\vec{E}^i = T\left(\vec{E}_\perp + \vec{E}_\parallel\right) = E_0\left(T_\perp \vec{e}_\perp + T_\parallel \vec{e}_\parallel\right)e^{-jkz}, \quad (2)$$

where $T_\perp$ and $T_\parallel$ are the vertical and horizontal transmission coefficient vectors, respectively. Then, the vertical and horizontal components experience two distinct phase shifts with the phase difference of 90 degrees while propagating through the converter. When satisfying the following conditions,

$$|T_\perp| = |T_\parallel|, \quad (3)$$

$$\Delta\varphi = \varphi_\perp - \varphi_\parallel = \pm 90^\circ. \quad (4)$$

As a result, within the transmission band, the polarization of the emerging wave on the other side will be circular.

2.2. Equivalent Circuit Model. To understand the principles of operation clearly, a simple equivalent circuit model is used to analyze this FSS structure as shown in Figure 2. The grids in the top and bottom metallic layers are modeled as the same parallel inductor (L_{x1} and L_{x3}), and the rectangular patches are modeled as the conductor C_{x2} in x direction and C_{y1}, C_{y2}, and C_{y3} in the y direction. The substrates separating these metal layers are represented by two short transmission lines with characteristic impedance of $Z_{i,i+1}, \ldots, Z_{N-1,N}$. For nonmagnetic media, $Z_{i,i+1} = Z_0\left(\varepsilon_r^{i,i+1}\right)^{-1/2}$, where ε_r is the dielectric constant of the substrate and $Z_0 = 377\ \Omega$ is the free space impedance, and length of $h_{1,2} = h_{2,3} = \lambda/8$ which is the substrate thickness and thickness of the F4B substrate is ignored, simplifying the circuit model. By adjusting these equivalent circuit values of the circuit, we could calculate the frequency of operation ($f_0 = 14.5$ GHz), operating bandwidth (BW), and the response type and order. And then these values would be mapped to the geometrical parameters of the proposed FSS structure.

2.3. Calculation Procedure. In the calculation procedure, to obtain the values of each elements of the equivalent circuit models shown in Figure 2. Firstly, we will determine all of the capacitor values. By using the values of capacitor, we can calculate the values of the equivalent inductor, respectively. For this FSS equivalent circuit shown in Figure 2, the first and the last capacitors could be calculated by using [13].

$$C_{y1} = \frac{q_1}{r_1\omega_0 Z_0\delta}, \qquad C_{y3} = \frac{q_3}{r_3\omega_0 Z_0\delta}, \quad (5)$$

where $\delta = \mathrm{BW}/f_0$ is the fractional bandwidth of the FSS and $\omega_0 = 2\pi f_0$ and r_1, r_3 are normalized source and load impedances ($r_1 = r_3 = 1$ when the FSS is surrounded by free space). Then, the value of the capacitor in middle layer is chosen such that

$$C_{y2} \le \frac{C_{y1}}{(\delta k_{1,2})^2}, \quad (6)$$

where $k_{1,2}$ is the normalized coupling coefficient between C_{y1} and C_{y3}. The inequality indicates that the choices

for the value of C_{y2} are not unique as long as it meets this condition.

After calculating the values of all the capacitors, the phase delay in y direction could be determined. According to the phase delay, to achieve 90 degrees phase difference between x and y direction, we should adjust the values of parameters in x direction to provide phase compensation. Thus, the inductors L_{x1} and L_{x3} can be determined as follows:

$$L_{x1} = \frac{1}{\omega^2\left(C_{y1} - k_{1,2}\delta\sqrt{C_{y1}C_{y2}}\right)},$$
$$L_{x3} = \frac{1}{\omega^2\left(C_{y3} - k_{2,3}\delta\sqrt{C_{y2}C_{y3}}\right)}. \quad (7)$$

To simplify the calculation process, we let C_{x2} meet the same condition (6). Up to now, all of the values of main parameters in equivalent circuit are determined as shown in Table 1. Based on the results, the values of structural parameters can be obtained as shown in Table 2.

According to these calculation results of structure parameters, simulation and optimization of the proposed structure have been carried out. Finally, a prototype of structure is fabricated and measured. We would prove the accuracy of our calculations in the next section.

3. Results and Analysis

3.1. Simulation Results. The simulation of the proposed FSS was carried out by using the commercial full-wave EM solver (CST Microwave Studio), and the results have been computed at normal incidence firstly. Figure 3(a) shows the simulated phase and phase difference between $E_{\parallel}^{\text{out}}$ and $E_{\perp}^{\text{out}}$. It can be seen that the phase difference (solid line) between $E_{\parallel}^{\text{out}}$ and $E_{\perp}^{\text{out}}$ is approximately 90 degrees, matching the condition (4). With regard to Figure 3(b), which shows the return loss and insertion loss of the reflection and transmission with normally incident LP wave, the polarizers provide a comparable magnitude of $E_{\parallel}^{\text{out}}$ and $E_{\perp}^{\text{out}}$, which matches the condition (3).

After analyzing the two conditions, the axial ratio (AR) could be calculated by [14].

$$\text{AR} = \sqrt{\frac{E_{\parallel}^2\cos^2\tau + E_{\parallel}E_{\perp}\sin 2\tau\cos\delta + E_{\perp}^2\sin^2\tau}{E_{\parallel}^2\sin^2\tau - E_{\parallel}E_{\perp}\sin 2\tau\cos\delta + E_{\perp}^2\cos^2\tau}}, \quad (8)$$

where δ is the phase difference between $E_{\parallel}^{\text{out}}$ and $E_{\perp}^{\text{out}}$ and τ is expressed by

$$\tau = \frac{1}{2}\tan^{-1}\left(\frac{2E_{\parallel}E_{\perp}}{E_{\parallel}^2 - E_{\perp}^2}\right). \quad (9)$$

Based on the results, the axial ratio of transmitted circularly polarized output wave is shown in Figure 3(c). For an axial ratio of less than 3 dB, the bandwidth is from 11.36 to 17.83 GHz, approximately 44.6% 3 dB AR bandwidth covering most of Ku-band. Within the whole AR < 3 dB bandwidth, the transmission coefficient is less than 1.5 dB between the 3 dB AR bandwidth.

During the optimization, the operating frequency could be changed via adjusting parameters of the middle patch, as shown in Figure 4(a). Generally, the size of patch has an effect on the value of equivalent conductor C_{x1} and C_{y2}. Therefore, the phase and magnitude responses for both perpendicular and parallel polarizations are changed, leading to the change of frequency response. The two responses can be calculated using the following formula [5]:

$$\Delta f_t \geq \frac{\Delta f_{\text{opt}}}{(1 - (\Delta\phi_{\text{d}}/\Delta\phi_t))}, \quad (10)$$

where Δf_t and $\Delta\phi_t$ are their frequency and phase shifts, Δf_{opt} is the operating bandwidth, and $\Delta\phi_{\text{d}}$ is the desired phase difference of 90° in an ideal situation.

Figure 4(b) shows the influence of parameters of top and bottom grid structure on bandwidth. H2 and H3 mainly control the length of vertical strips which couple capacitively. Therefore, they affect the value of conductor C_{y1} and C_{y3}. When increasing the length of grid strips, the bandwidth becomes narrow due to the influence on the loss of parallel-direction electric field only, which results in unequal amplitudes in parallel and perpendicular directions. Consequently, the axial ratio deteriorates.

On the other hand, although the bandwidth (H2 = 4.8 mm and H3 = 3.6 mm) is wider than the bandwidth (H2 = 5.1 mm and H3 = 3.9 mm) in the condition of normal incidence, we choose the parameters of H2 = 5.1 mm and H3 = 3.9 mm considering different oblique incidence. Here are the simulated and experimental axial ratio results for oblique incidences in Figure 5.

3.2. Analysis on Oblique Incidence and Experimental Results. It can be seen from Figures 5(a) and 5(b) that with the increasing of oblique incidence, the 3 dB AR bandwidth becomes narrow which is a common trend. Leading to the deterioration of axial ratio is that in condition of large oblique incidence, the transmitted wave hardly meets the conditions (3) and (4). However, the proposed polarization converter still shows a good performance in case of 50 degrees oblique incidence in both x-z and y-z planes. Therefore, the maximum of oblique incidence angle is 50 degrees.

The experimental results are shown in Figures 5(c) and 5(d). The measurement procedure and photograph of the fabricated polarizer converter are shown in Figure 6. The measured frequency is set from 11 GHz to 19 GHz. Due to the limited operating bandwidth of the standard-gain horn used (Ku-band horn, operating in 12–18 GHz), it would cause the deterioration in low and high frequency. From the results, we can see that there is a good consistency

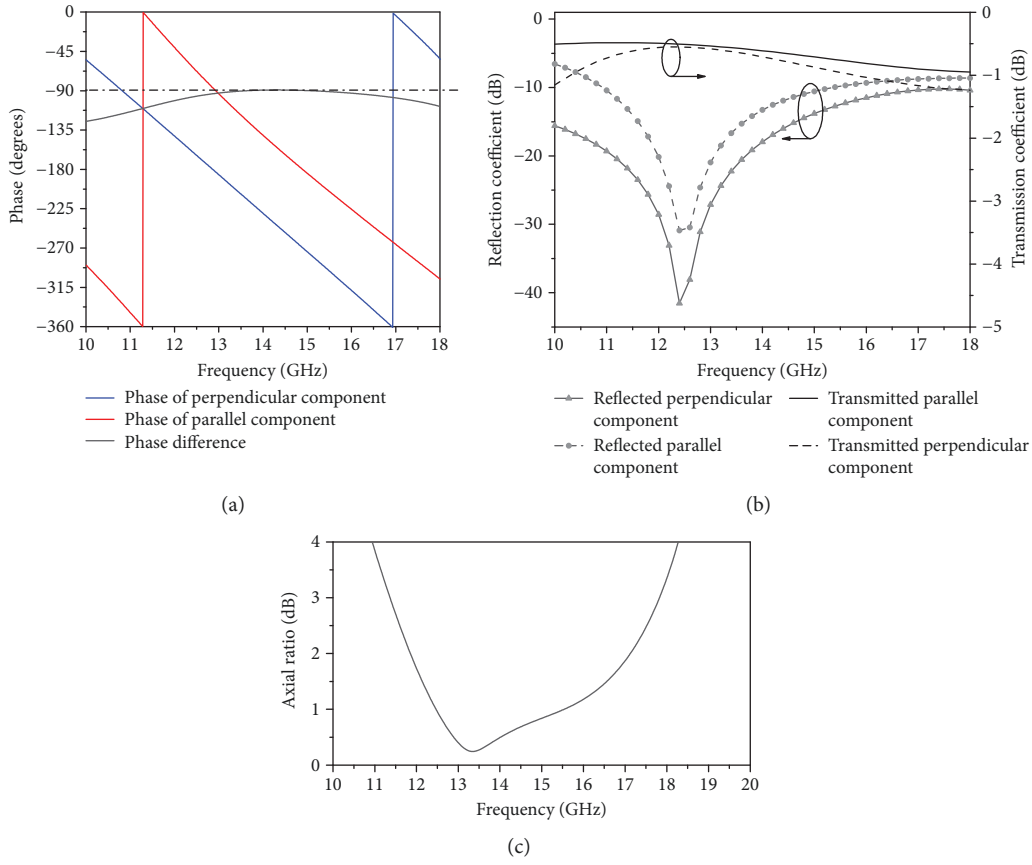

Figure 3: The simulation results of the proposed FSS structure. (a) The phase relation between output wave in perpendicular and parallel direction. (b) The transmission and reflection coefficients. (c) The axial ratio of proposed FSS under normal incidence.

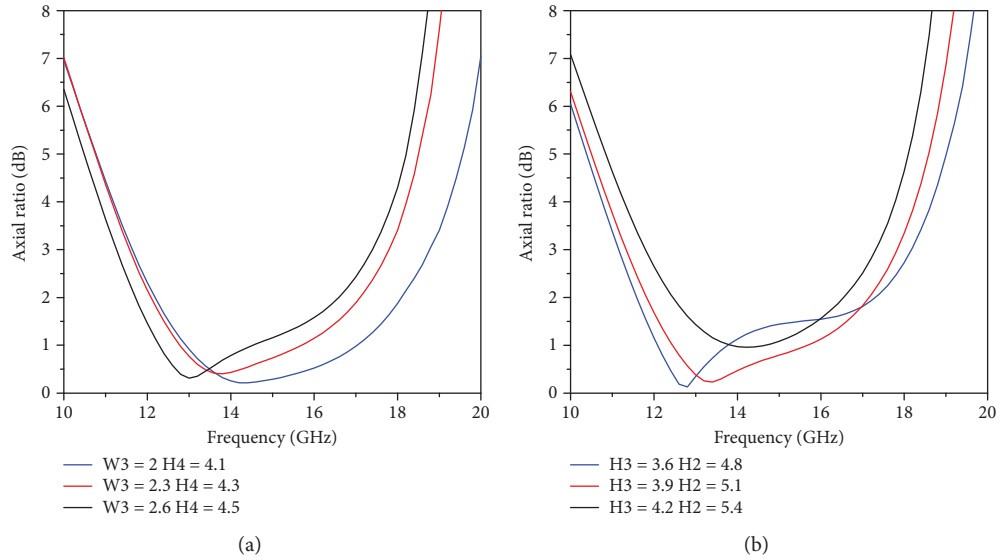

Figure 4: Simulated axial ratio of the proposed FSS for different (a) parameters of middle patch structure and (b) parameters of top and bottom grid structure.

between the experimental and simulated results, despite the instability in axial ratio and the shift in frequency. These deviations may be caused by the manufacturing errors and the experimental environment.

The simulated and measured transmission and reflection coefficient results are shown in Figure 7 which demonstrate that during the whole 3 dB AR bandwidth, the peak loss is less than 1.5 dB.

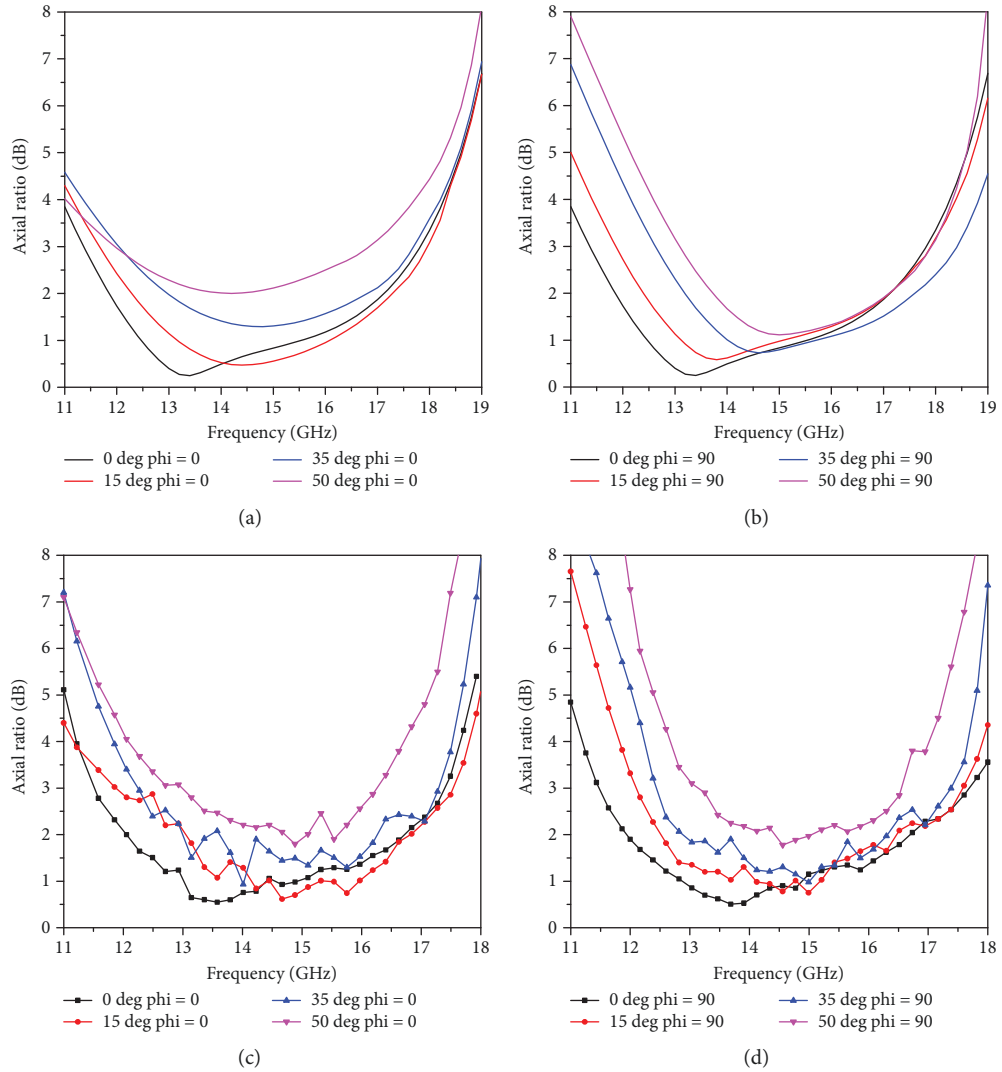

Figure 5: Simulated (a, b) and experimental (c, d) axial ratio results for oblique incidences of 0, 15, 35, and 50 degrees in (a) x-z and (b) y-z planes.

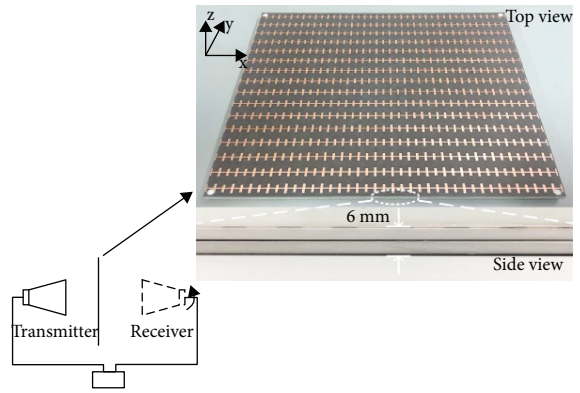

Figure 6: The measurement procedure and two views (top and side views) of the fabricated polarization converter.

The comparison between our design and some typical published polarizers is shown in Table 3 and these data are based on simulation due to some designs are not fabricated and measured. Contrast with single- and multilayer-layer design, the polarizer we proposed has advantages in bandwidth and peak loss.

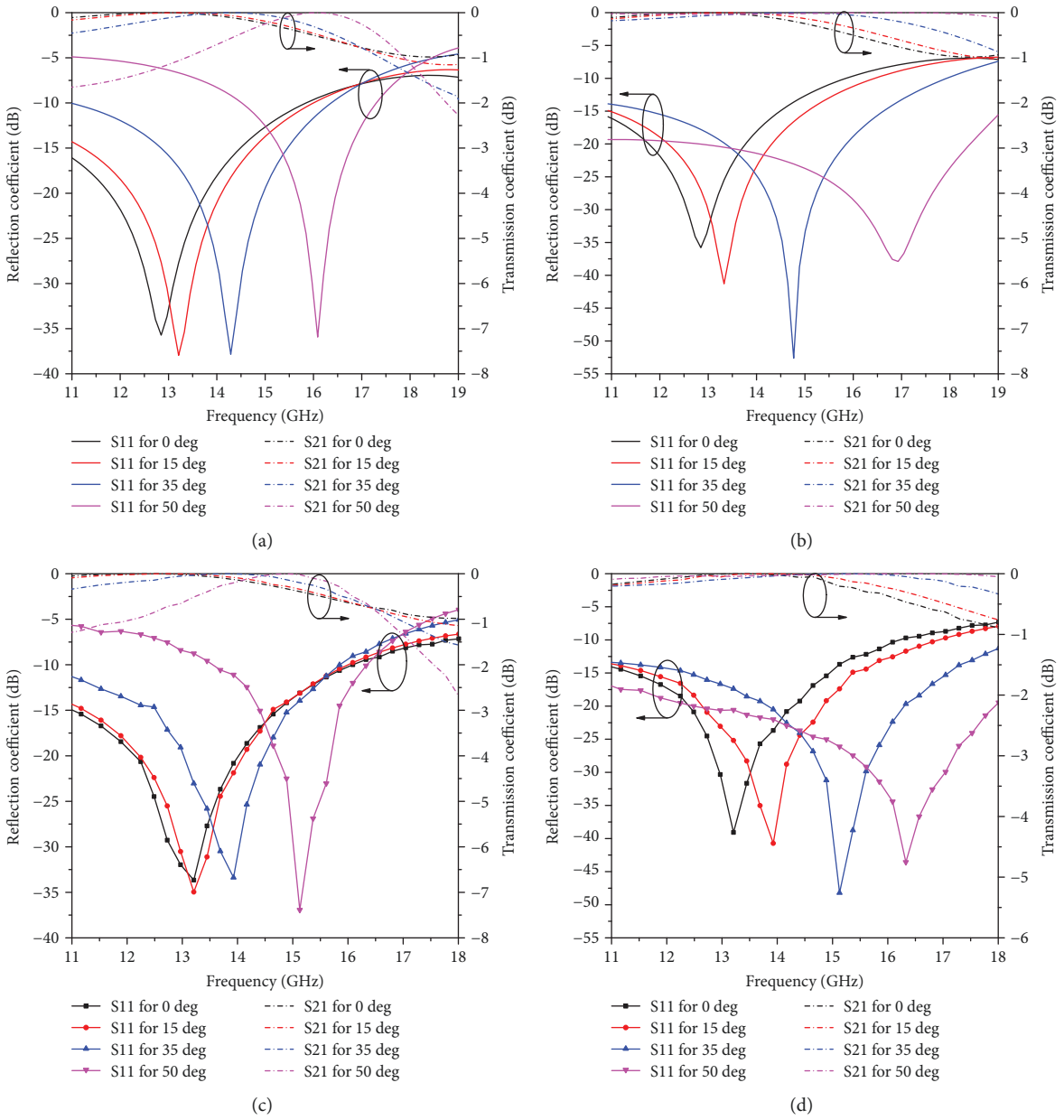

Figure 7: Simulated (a, b) and experimental (c, d) transmission and reflection coefficient results for oblique incidences of 0, 15, 35, and 50 degrees in (a, c) x-z and (b, d) y-z planes.

Table 3: Comparisons between the proposed structure and some other reported linear-to-circular polarizer.

Ref. work	Layer	Bandwidth	Oblique performance
[3]	1	21%	N/A
[10]	3 (0.31λc)	40.5%	±45
[11]	3 (0.33λc)	>35%	±45
[5]	5	40%	±45
[6]	5	19.6%	±50
[7]	5	4.8%	±70
Our work	3 (0.28λc)	44.6%	±50

4. Conclusion

In this communication, we present a three-layer linear-to-circular polarizer based on grid-patch structure for Ku-band. The equivalent circuit model theory is used to analyze the operating principle of this periodic structure and the design process is given. Simulation, optimization, and measurement have been carried out. The proposed structure shows a good performance on thickness (0.28λc) and bandwidth (44.6%). Besides, this design could be also applied to beam scanning antennas because of its capability in condition of large oblique incidence angle (±50 deg).

Data Availability

The data used to support the findings of this study are available from the corresponding author upon request.

Conflicts of Interest

There is no conflict of interest regarding the publication of this paper.

References

[1] J.-M. Wu, X. Lei, D.-f. Zhou, L. Hou, and H.-w. Chen, "Design of ring-focus elliptical beam reflector antenna," *International Journal of Antennas and Propagation*, vol. 2016, Article ID 9615064, 7 pages, 2016.

[2] P. Fei, Z. Shen, X. Wen, and F. Nian, "A single-layer circular polarizer based on hybrid meander line and loop configuration," *IEEE Transactions on Antennas and Propagation*, vol. 63, no. 10, pp. 4609–4614, 2015.

[3] M. Euler, V. Fusco, R. Dickie, R. Cahill, and J. Verheggen, "Sub-mm wet etched linear to circular polarization FSS based polarization converters," *IEEE Transactions on Antennas and Propagation*, vol. 59, no. 8, pp. 3103–3106, 2011.

[4] J.-m. Wu, D.-f. Zhou, X. Lei, J. Gao, and H.-m. Hu, "Design of a compact broadband 90° waveguide twist based on double-corner-cut square slots," *International Journal of Antennas and Propagation*, vol. 2017, Article ID 8657620, 5 pages, 2017.

[5] S. M. A. Momeni Hasan Abadi and N. Behdad, "Wideband linear-to-circular polarization converters based on miniaturized-element frequency selective surfaces," *IEEE Transactions on Antennas and Propagation*, vol. 64, no. 2, pp. 525–534, 2016.

[6] D. Blanco and R. Sauleau, "Broadband and broad-angle multilayer polarizer based on hybrid optimization algorithm for low-cost Ka-band applications," *IEEE Transactions on Antennas and Propagation*, vol. 66, no. 4, pp. 1874–1881, 2018.

[7] T. Dousset, A. Bellion, I. Le Roy, and G. Morvan, "Polariseurs circulaires'a m'eandres pour applications spatiales," in *18'emes Journ'ees Nationales Microondes*, pp. 15–17, Paris, France, 2013.

[8] E. Arnaud, R. Chantalat, M. Koubeissi, T. Monediere, E. Rodes, and M. Thevenot, "Global design of an EBG antenna and meander-line polarizer for circular polarization," *IEEE Antennas and Wireless Propagation Letters*, vol. 9, pp. 215–218, 2010.

[9] L. Sun and A. Zaghoul, "Two-layer wide-band *meander*-line-polarizer," US Patent http://www.google.ch/patents/US20050104791, 2005.

[10] C. Pfeiffer and A. Grbic, "Millimeter-wave transmitarrays for wavefront and polarization control," *IEEE Transactions on Microwave Theory and Techniques*, vol. 61, no. 12, pp. 4407–4417, 2013.

[11] M.-A. Joyal and J.-J. Laurin, "Analysis and design of thin circular polarizers based on meander lines," *IEEE Transactions on Antennas and Propagation*, vol. 60, no. 6, pp. 3007–3011, 2012.

[12] J. Gao, X. Lei, G.-H. Chen, Y. Zhang, and J.-M. Wu, "Design of the variable inclination continuous transverse stub antenna based on rectangular grating slow-wave structure," *International Journal of Antennas and Propagation*, vol. 2018, Article ID 5793535, 7 pages, 2018.

[13] N. Behdad and M. A. al-Joumayly, "A generalized synthesis procedure for low-profile frequency selective surfaces with odd-order band-pass responses," *IEEE Transactions on Antennas and Propagation*, vol. 58, no. 7, pp. 2460–2464, 2010.

[14] N. Li and Y. Feng, "Fast measuring axial ratio of circular polarization antennas based on linear polarization antenna," *Infrared and Laser Engineering*, vol. 42, no. 8, pp. 2216–2220, 2013.